Mapping surficial sediments in the Interior Plateau using remotely piloted aircraft system lidar

E.A. Elia
T. Ferbey
B.C. Ward

BRITISH COLUMBIA
Ministry of
Energy, Mines and
Low Carbon Innovation

Open File 2024-03

Ministry of Energy, Mines and Low Carbon Innovation
Responsible Mining and Competitiveness Division
British Columbia Geological Survey

Recommendation citation: Elia, E.A., Ferbey, T., and Ward, B.C., 2024. Mapping surficial sediments in the Interior Plateau using remotely piloted aircraft system lidar. British Columbia Ministry of Energy, Mines and Low Carbon Innovation, British Columbia Geological Survey Open File 2024-03, 12p.

Front cover:
DJI Matrice 600 Pro aircraft mounted with a Green Valley LiAirV70 facing away from the camera at a height of approximately 30 m above ground level. **Photo by Katya Zaborniak**.

Back cover:
DJI Matrice 600 Pro aircraft mounted with a Green Valley LiAirV70 landed on a forestry road at survey area 21TFE0002. Cases in background house aircraft batteries, LiAir V70 sensor and laptop for lidar processing. **Photo by Travis Ferbey**.

BRITISH COLUMBIA

Ministry of
Energy, Mines and
Low Carbon Innovation

Mapping surficial sediments in the Interior Plateau using remotely piloted aircraft system lidar

E.A. Elia
T. Ferbey
B.C. Ward

Ministry of Energy, Mines and Low Carbon Innovation
British Columbia Geological Survey
Open File 2024-03

Mapping surficial sediments in the Interior Plateau using remotely piloted aircraft system lidar

E.A. Elia[1,2a], T.Ferbey[1], and B.C. Ward[2]

[1] British Columbia Geological Survey, Ministry of Energy, Mines and Low Carbon Innovation, Victoria, BC, V8W 9N3
[2] Department of Earth Sciences, Simon Fraser University, Burnaby, BC, V5A 1S6
[a] corresponding author: easton.elia@gov.bc.ca

Recommendation citation: Elia, E.A., Ferbey, T., and Ward, B.C., 2024. Mapping surficial sediments in the Interior Plateau using remotely piloted aircraft system lidar. British Columbia Ministry of Energy, Mines and Low Carbon Innovation, British Columbia Geological Survey Open File 2024-03, 12p.

Abstract
Remotely piloted aircraft systems (RPAS) and the sensors they carry enable rapid collection and processing of high-resolution lidar data at low cost. We used a commercially available RPAS to collect lidar data at 80 to 100 m above ground level to build digital elevation models at resolutions of up to 0.25 m over areas <1.3 km² in heavily drift covered parts of the Interior Plateau, near the Woodjam and Mount Polley deposits and in the Guichon Creek batholith. The elevation models and derived hillshade models enabled 1:5,000-scale surficial geology mapping in which features that might otherwise be masked by dense forest canopies could be recognized. Landforms and units as small as ~100 m² that exhibit subtle surface expressions and cannot be identified on traditional <1:20,000-scale air photos or from ground observations can be mapped using RPAS lidar.

Keywords: remotely piloted aircraft system, lidar, GreenValley International LiAir V70, ice flow history, till, surficial geology mapping, Interior Plateau, digital elevation model

1. Introduction

Historically, surficial geology mapping has relied heavily on air photo interpretation. Although air photos will remain a useful standard mapping tool, detail is reduced in forested terrain where surface features are commonly masked by vegetation. Deposits that display subtle relief changes like glaciofluvial gravels and streamlined tills are particularly difficult to map through treed areas. Furthermore, although many decades of air photos acquired during fixed-wing aircraft missions flown by provincial and federal agencies can be purchased (currently $18.50/frame, British Columbia Ministry of Forests, 2023), acquiring current air photos with new flight missions for a specific project may be cost prohibitive. Light detection and ranging (lidar) scanners mounted to helicopters or fixed-wing aircraft can acquire accurate, high-resolution elevation values which can be used to generate digital elevation models (DEMs) and help resolve mapping difficulties in heavily treed areas. However, project-specific lidar acquisition may also be cost prohibitive (~$250/km^2), and mappers typically only use lidar products when they have been made publicly available such as by the British Columbia Ministry of Water, Land and Resource Stewardship (LidarBC, 2024) or collected for other purposes (Demchuk et al., 2005). The emergence of miniaturized lidar sensors mounted on remotely piloted aircraft systems may offer low-cost solutions for some mapping projects, particularly those needing near-real time imagery of the Earth's surface.

In 2019, the British Columbia Geological Survey started a project to assess applying RPAS to surficial geology mapping and drift prospecting. The project began with a small, consumer quadcopter RPAS to fly air photo missions and produce photogrammetric DEMs for an area in north-central British Columbia (Elia and Ferbey, 2020). The project evolved to using a larger RPAS hexacopter with external payloads to evaluate RPAS-borne sensors to map and characterize the composition of surficial sediments in the Interior Plateau (Elia et al., 2023). This second phase of the program, conducted during the summers of 2021 and 2022, focussed on RPAS lidar, air photo, magnetic, and radiometric autopilot surveys at 13 sites. Elia et al. (2023) presented the complete geophysics and geomatics datasets collected and, for each sensor, how the data were acquired and processed. In this report, we use a subset of the lidar data to assess the utility of high spatial resolution, field-generated, DEMs and hillshade models to map surficial geology in the Interior Plateau (Fig.1).

2. Setting

We conducted RPAS lidar surveys in the Woodjam (Sausser Lake), Mount Polley, and Guichon Creek batholith (Skuhost Creek, Spaist Mountain) areas (Fig. 1). Topography across the Interior Plateau is subdued, with ubiquitous drift cover and isolated bedrock exposures (Holland, 1976). The Interior Plateau is underlain by rocks of Stikine and Quesnel terranes with high potential for porphyry mineral system deposits and hosts producing alkalic (Cu-Au) porphyry mines (e.g., Mount Polley, Mount Milligan, Copper Mountain, New Afton), calc-alkaline (Cu-Mo) porphyry mines (Gibraltar, Highland

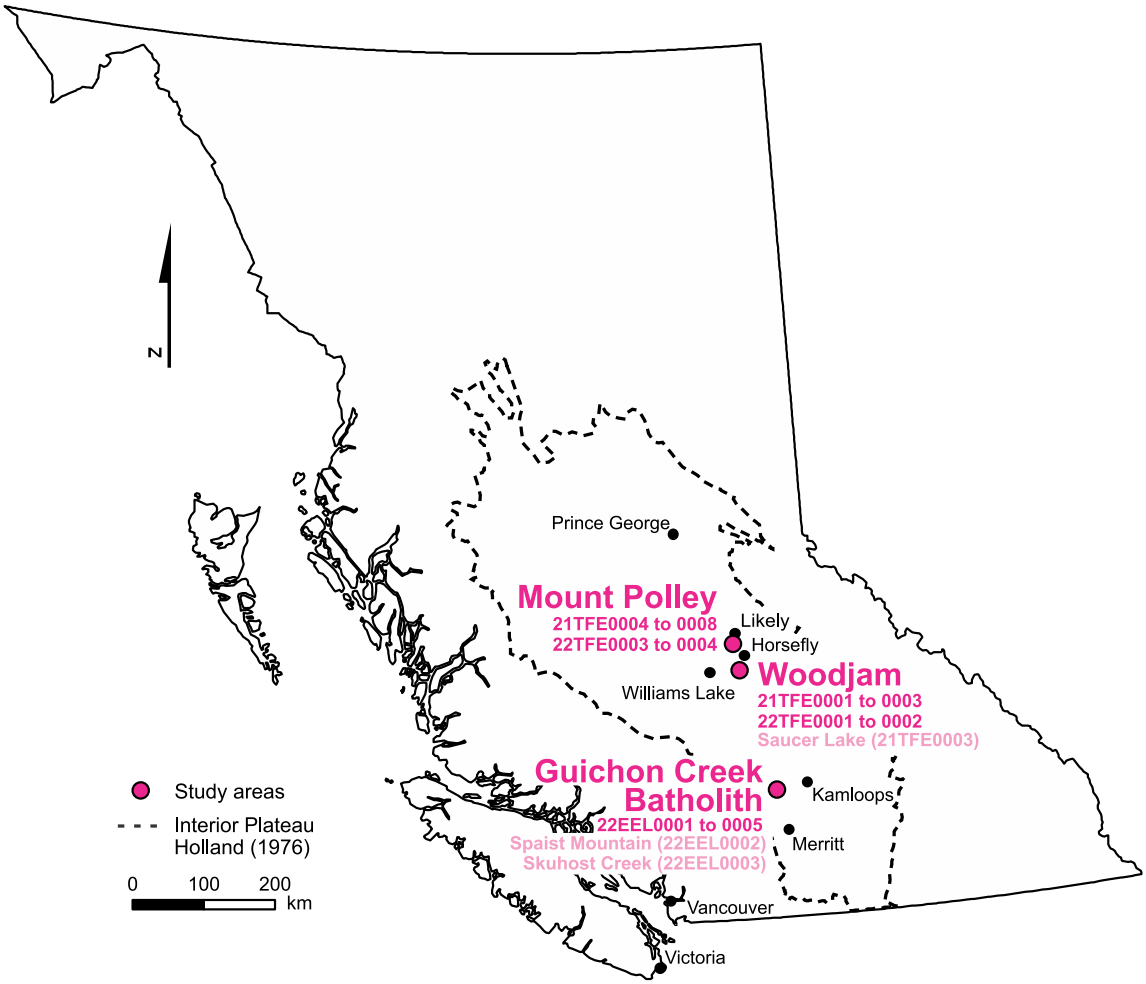

Fig. 1. Study area locations.

Valley), and numerous past-producing mines and mineral occurrences (e.g., Logan, 2013). Each of the study areas has extensive forest-service road networks and recent logging has produced harvested areas devoid of most large (>10 m tall) trees (cutblocks).

During the Late-Wisconsinan, the Cordilleran ice sheet was at its maximum extent and completely covered the Interior Plateau (Clague and Ward, 2011). At this time, ice flowed from a divide at 52° north latitude independent of topography, contributing to well-defined ice flow to the west-northwest at Horsefly and Mount Polley and south-southeast at the Guichon Creek batholith (Plouffe and Ferbey, 2016). Tills are the predominant surficial material across the Mount Polley, Horsefly, and Guichon Creek study areas and subglacial tills in the form of till veneers (<2 m thick), till blankets (>2 m thick), and streamlined tills are common (Hashmi et al., 2015a; Ferbey et al., 2016; Plouffe and Ferbey, 2018). Mineral exploration is hampered by extensive sediment cover, knowledge about the surficial geology of the region is needed to find bedrock outcrop, evaluate geochemical and geophysical results, conduct drift prospecting, and better understand known mineral occurrences (Diakow et al., 1997; Kerr and Levson, 1997; Plouffe and Ferbey, 2017).

3. Methods

Lidar scanners emit high-frequency laser pulses and measure the return times of multiple reflections from horizontal or vertical surfaces (dictated by instrument orientation and field of view or FOV) that are assigned x, y, and z coordinates (Lemmens, 2007; Lohani and Ghosh, 2017; Nayegandhi and Nimetz, 2018). Spatially referenced points are viewed as a point cloud that can be classified and separated based on return times (or z values). Over treed areas, early returns are reflected off the upper tree canopy whereas later returns reflect off the ground surface (Maune et al., 2018). This provides lidar with the ability to see through forests and low-lying vegetation to create bare-Earth DEMs, which are representations of the Earth's surface devoid of vegetation. Hillshade models are three-dimensional grey-scale representations of the terrain that are produced from bare-Earth DEMs by simulating the effects of illumination from specific angles and azimuths.

3.1. Instrumentation and procedure

We used a GreenValley International LiAir V70 mounted to a DJI Matrice 600 Pro (M600) RPAS to collect lidar data (Fig. 2). Details on the LiAir V70, M600, and specific survey parameters (e.g., flight height, speed, line spacing) are presented in Elia et al. (2023). The LiAir V70 uses a Livox AVIA sensor

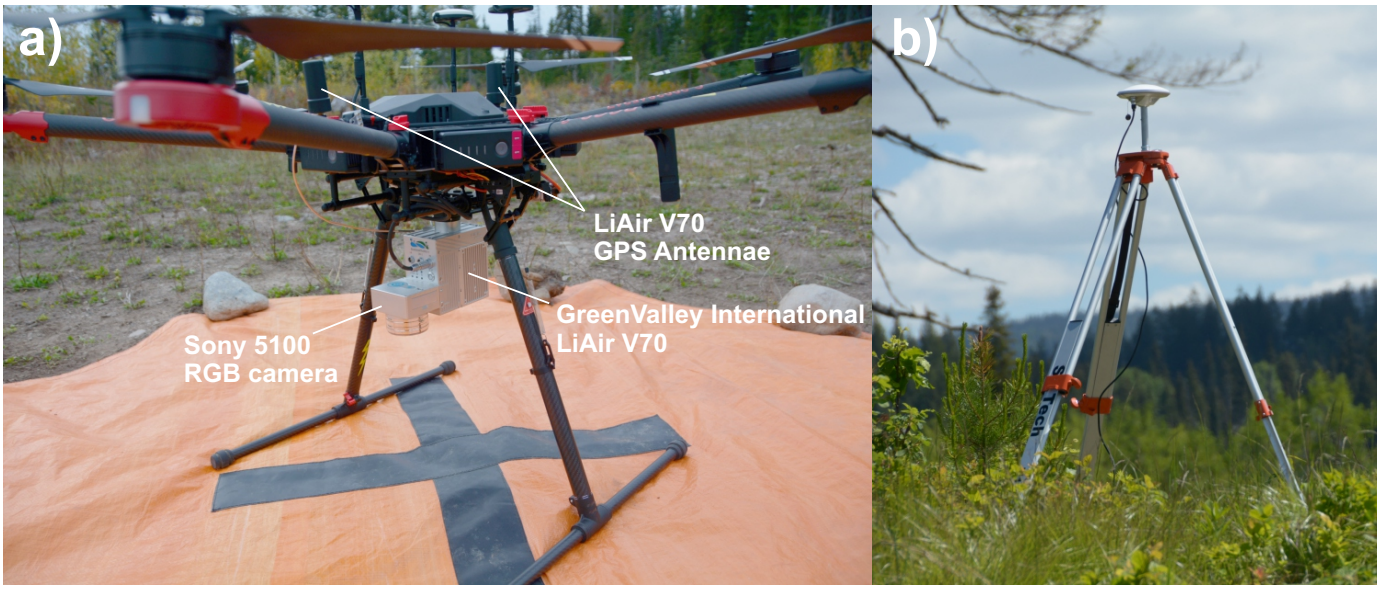

Fig. 2. RPAS platform and lidar scanner. **a)** Green Valley LiAir V70 (including RGB camera module) mounted on a DJI Matrice 600 Pro aircraft. The two LiAir V70 external global navigation satellite system antennae are mounted to the top of the aircraft. **b)** LiAir V70 global navigation satellite system base station.

to acquire lidar data and a built-in Sony A5100 RGB camera to simultaneously capture colour photographs (Table 1). The Livox AVIA emits 240,000 laser pulses/s and receives up to three returns (720,000 pulses/s) using a horizontal field of view of 70.4° (GreenValley International, 2017). The Sony A5100 is a 24.3 megapixel, mechanical shutter, APS-C, CMOS camera used to capture RGB imagery at a similar horizontal field of view as the Livox sensor. The LiAir V70 uses two global navigation satellite system (GNSS) antennae mounted to the top of the aircraft that detect signals from GPS, GLONASS, GALILEO and BeiDou constellations (GreenValley International, 2017). Although powered by the LiAir M600 batteries, during data collection the LiAir V70 operates independently and does not communicate with the M600. Most of our flights required more than one M600 battery change to complete. For the 2021 surveys, battery changes were completed by powering down both the LiAir M600 and LiAir V70. However, doing so necessitated repeating the LiAir V70 initialization and calibration procedures. So, in 2022, we hot-swapped the M600 batteries without interrupting power to the LiAir V70 so that the survey could be resumed immediately after take-off. Including battery changes, set-up, and tear-down, lidar surveys can take up to 3 hours to conduct in the field, with ~20 minutes of flight time per battery set.

A GreenValley International global navigation satellite system base station recorded spatial correction data during, 10 minutes before, and 10 minutes after lidar acquisition. During the initial 10-minute calibration of the base station, we powered on the LiAir V70 and set its instrument parameters using proprietary software running on a laptop. Flying height and line spacing were calculated using the 70.4° horizontal FOV of the LiAir V70, as suggested by Alsadik and Remondino (2020), and a 50% swath overlap between adjacent flight lines. For all surveys, the aircraft was configured to fly at 4-5 m/s and 80-100 m above ground level (Table 1). Photo settings were set to capture a photo every 2 s after reaching heights >50 m above ground level. Once airborne, a 'figure 8' flight pattern was completed to calibrate the scanner before the survey was initiated; an additional figure 8 was flown before landing.

The primary criteria used to select the survey areas were that they had to be underlain by subglacial till, be centred on a flyable cutblock, and have existing geological, geochemical, and geophysical datasets to assess instrument performance (Elia et al., 2023; Ferbey et al., 2024).

3.2. Data processing

RPAS-lidar data were first downloaded from the instrument and imported into LiGeoreference (v. 1.4.0) where we aligned the lidar and base station data, colourized the point cloud using the RGB photos, removed outlier and cornering points, and aligned data to each flight line (Fig. 3; see Elia et al., 2023 for details). For the data presented here, we used Cloud Compare's (v. 2.13) cloth simulation filtering (CSF Filter) tool to classify and separate ground points to create bare-Earth DEMs (Zhang et al., 2016). Ground point density was calculated using the Cloud Compare geometric features calculator (surface density) with a radius of 0.56 m (1 m^2 circular area). DEM hillshading was performed in ArcMap (v. 10.8.1) with illumination parameters adjusted to emphasize specific features in the DEM. We processed all data in the field using a laptop computer with a 2.2 GHz Intel Core i7 CPU, 32 GB RAM, and an NVIDIA Quadro P3200 graphics card. The time required for data processing (i.e., producing a DEM or hillshade model from raw lidar data) depended on the size of the captured area and was usually equivalent to the time required for data acquisition.

3.3. Mapping surficial geology

We mapped manually in ArcMap primarily using RPAS lidar DEMs and hillshade models. To provide context, we supplemented RPAS lidar products with orthomosaics generated from air photos acquired by a DJI Phantom 4 RTK (Elia et al., 2023). Map units and landforms were defined and

Table 1. Technical parameters of the Green Valley LiAir V70 lidar sensor.

Parameter	Aircraft, instrument, and survey specifications
Aircraft platform	DJI Matrice 600 Pro
Instrument	GreenValley International LiAir V70
Sensor Type	70.4-degree field of view, Livox AVIA lidar sensor with 24.3 MP mechanical shutter camera
Instrument size	17.8 x 8.2 x 14.0 cm
Instrument weight	1.1 kg
Flying height	80 to 100 m above ground
Flying speed	4 m/s
Products	Colourized point cloud, digital elevation model
Scan rate	240,000 pts/s (first returns)
Spatial resolution*	25 cm/pixel*

*Resolution is based on a range of parameters and constraints including flying height, speed, overlaps, computer hardware, and desired processing time.

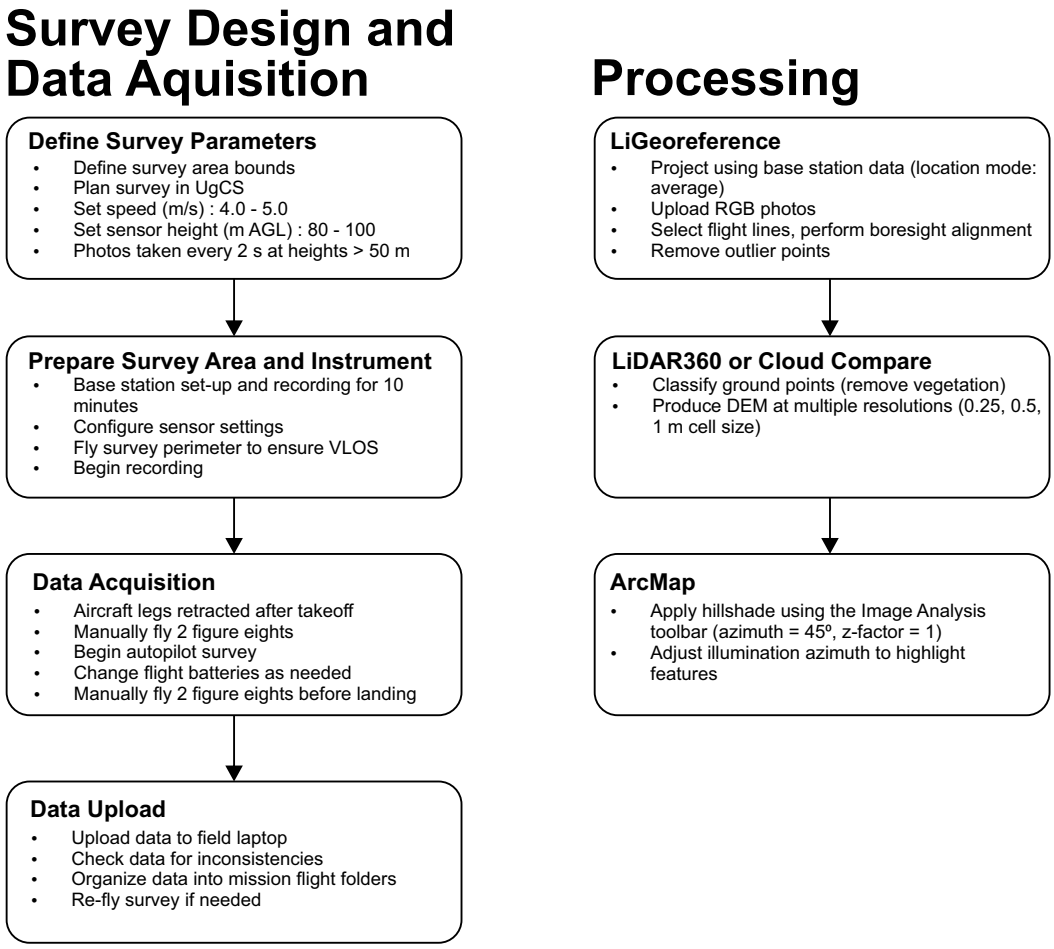

Fig. 3. Workflow for RPAS-lidar data acquisition and generation of lidar DEMs and hillshade models.

classified based on standards from Deblonde et al. (2019). Each RPAS survey site was visited, and a pit (<1 m deep) was dug in a centrally located till unit to test for subglacial till and collect samples for geochemical and mineralogical analysis. Exposed bedrock outcrop within, or directly adjacent to, the survey area was investigated for ice-flow indicators. No other detailed observations related to surficial geology classification were made in the field. The presented mapping is based on observations made in RPAS air photos and lidar products alone.

4. Results

We present results from multiple lidar missions flown in 2021 and 2022 with a focus on one, 21TFE0003 (Sausser Lake), in the Horsefly area (Fig. 1).

4.1. Acquisition and model production

The point cloud generated for Sausser Lake has an average ground point density of 721 pts/m^2. Ground point density can vary greatly depending on the forest and vegetation conditions and survey parameters, contributing to the observed ground point density standard deviation of 411 pts/m^2 across the entire point cloud (Fig. 4). In areas of swath overlap, parallel to flight lines, point density doubles. For example, the Sausser Lake site has densities of ~950 pts/m^2 in overlapping swaths, whereas areas of no overlap have densities of ~450 pts/m^2. In addition to swath overlap, we observed a pattern perpendicular to flight lines, produced by the physical back-and-forth scanning motion of the lidar sensor (scan lines). This pattern produces areas of higher-density data where the scan lines overlap (Fig. 4). The maximum density of ~3000 pts/m^2 only appears in specific, small areas of overlapping swaths and multiple scan lines. Depending on the software used to classify ground points and the prespecified spatial resolution of the DEM, the point cloud may be sub-sampled, resulting in point densities as low as 16 pts/m^2 to create DEMs with spatial resolutions of 0.25 m. Elia et al. (2023), show a subsampled ground point cloud of 79 pts/m^2 at another site (21TFE0002, Woodjam, Fig. 1) that supports a cell size of 0.25 m.

The lidar instrument can measure the trees, ground cover, and the ground surface in forest stands. The number of lidar pulses that reach the ground depends on the tree canopy thickness with foliage and solid objects (e.g., boughs, tree trunks) reducing the ground point density (Fig. 4). The density of ground points decreases toward the centre of dense forest stands as a result. In these areas, second and third returns are more indicative of the ground surface compared to the first returns, which commonly represent the upper portions of the tree canopy. Because lidar cannot penetrate through solid objects, ground point density reduces to zero where tree trunks or branches reflect the full laser pulse and prevent it from reaching the ground surface. The ground point classification process also excludes large boulders (marked by steep changes in topography) and produces no-data voids in their place. First returns representing the ground surface can still be found in some dense forest stands due to the low flight height (~80 m above ground level) and high horizontal field of view (70.4°) of the lidar instrument enabling pulses to travel obliquely beneath the tree canopy unobstructed (Fig. 4).

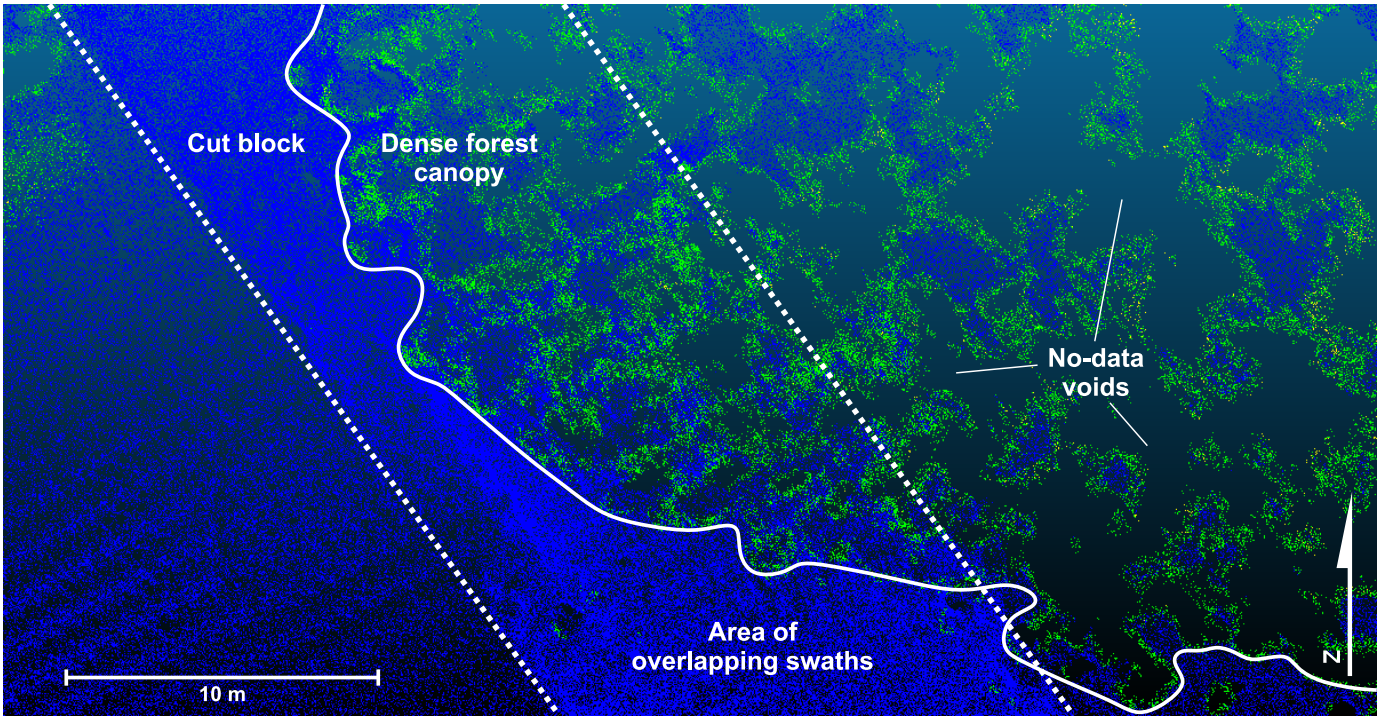

Fig. 4. Lidar ground-classified point cloud at site 22EEL0003 (Skuhost Creek). Only points classified as the ground using Cloud Compare's cloth simulation filtering tool (CSF tool; Zhang et al., 2016) are shown. Points are coloured based on return number, with blue points representing first returns, green points representing second returns, and yellow points (rare) representing third (last) returns. The number of second- and third-return ground points increases in the forested region (east of solid white line). Ground points are absent in the areas with the densest forest canopy. In the southwest corner are northeast-trending linear data artifacts that are perpendicular to flight line azimuth and related to acquisition.

Bare-Earth DEMs produced from the point clouds mostly show topographic changes that result from changes in geomorphology and surficial geology (Fig. 4). These DEMs may also show objects such as boulders, stumps, and fallen trees or artifacts related to data acquisition or processing (Fig. 5c, 5d). Long grasses, shrubs, and remaining standing trees in the cutblock may scatter lidar pulses and cause vertical inaccuracies that cannot be attributed to a single feature. Due to the no-data voids produced by trunks of standing trees, we locally see slight textural differences where the dense trees begin: the no-data voids produce circular areas with smooth, less detailed surface textures (Fig. 6). Dense forest stands with few separated ground points lead to the hillshade model displaying less detail than surrounding areas (Fig. 6). Nonetheless, the model still accurately represents the ground surface.

4.2. Resolvable features at multiple spatial resolutions

DEMs were produced using the same point cloud and techniques at varied spatial resolutions (1 m, 0.5 m, 0.25 m, and 0.1 m) to determine the appropriate resolution for delineating areally small surficial features. The four hillshade models (different resolutions) use the same illumination parameters over the same part of the Sausser Lake site (Fig. 5). The 1 m resolution version (Fig. 5a) is pixelated and appears blurred compared to the other higher-resolution versions. The mappable features in this DEM include 2-3 m wide, ~1 m deep drainage ditches. Adjacent to these features, the ground surface is relatively smooth and does not depict variation recognizable as changes in geomorphology or low-lying vegetation. In the northeast part of the figure, a southeast-sloping embankment is visible, although it cannot be followed to the south. As

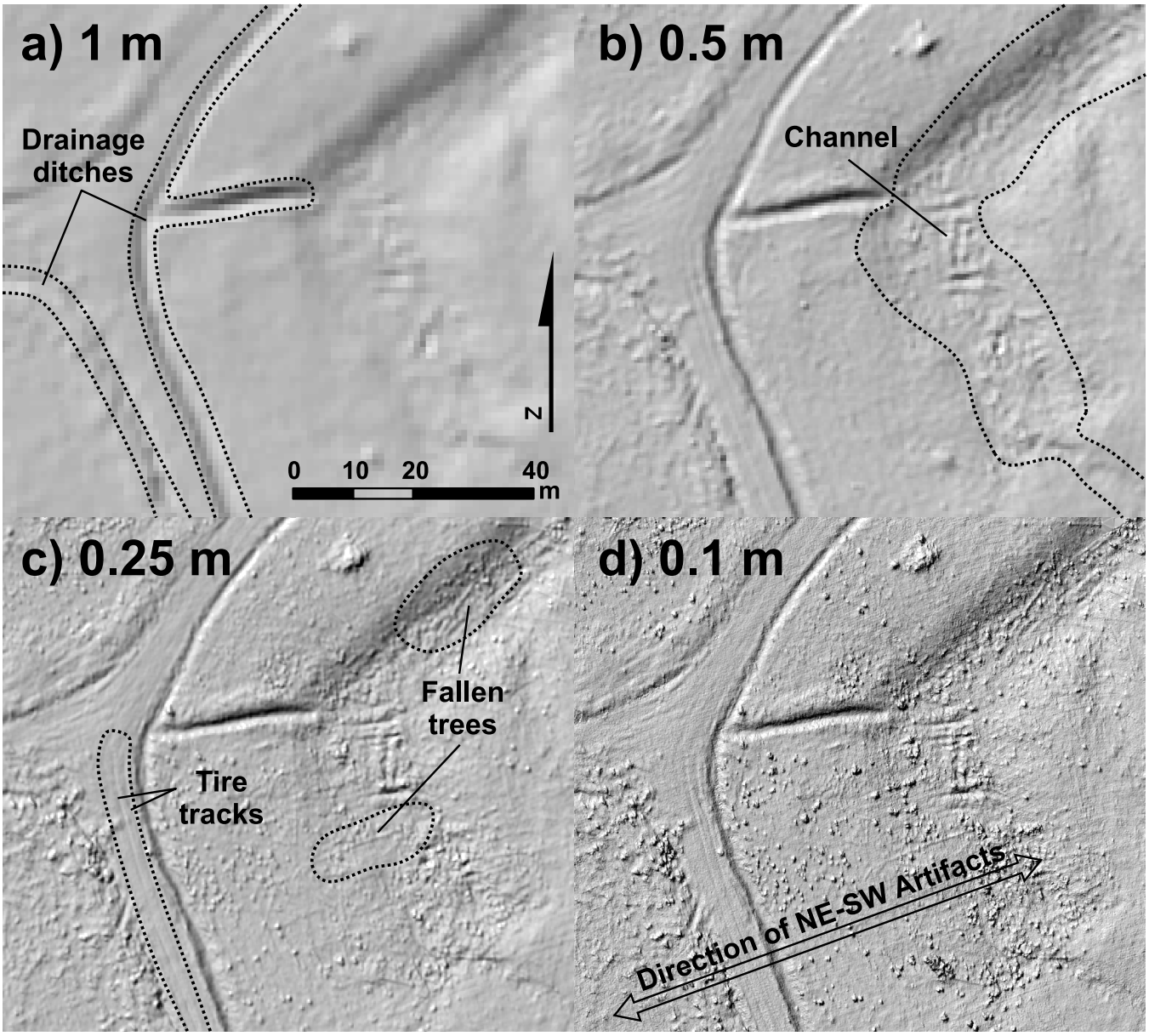

Fig. 5. Comparison of RPAS lidar products at increasing spatial resolutions. Hillshade models from 21TFE0003 (Sausser Lake) produced in Cloud Compare using an illumination azimuth of 315° and an altitude (angle of Sun above the horizon) of 45° at spatial resolutions of **a)** 1 m, **b)** 0.5 m, **c)** 0.25 m, and **d)** 0.1 m. Resolvable features are indicated with black dotted outlines.

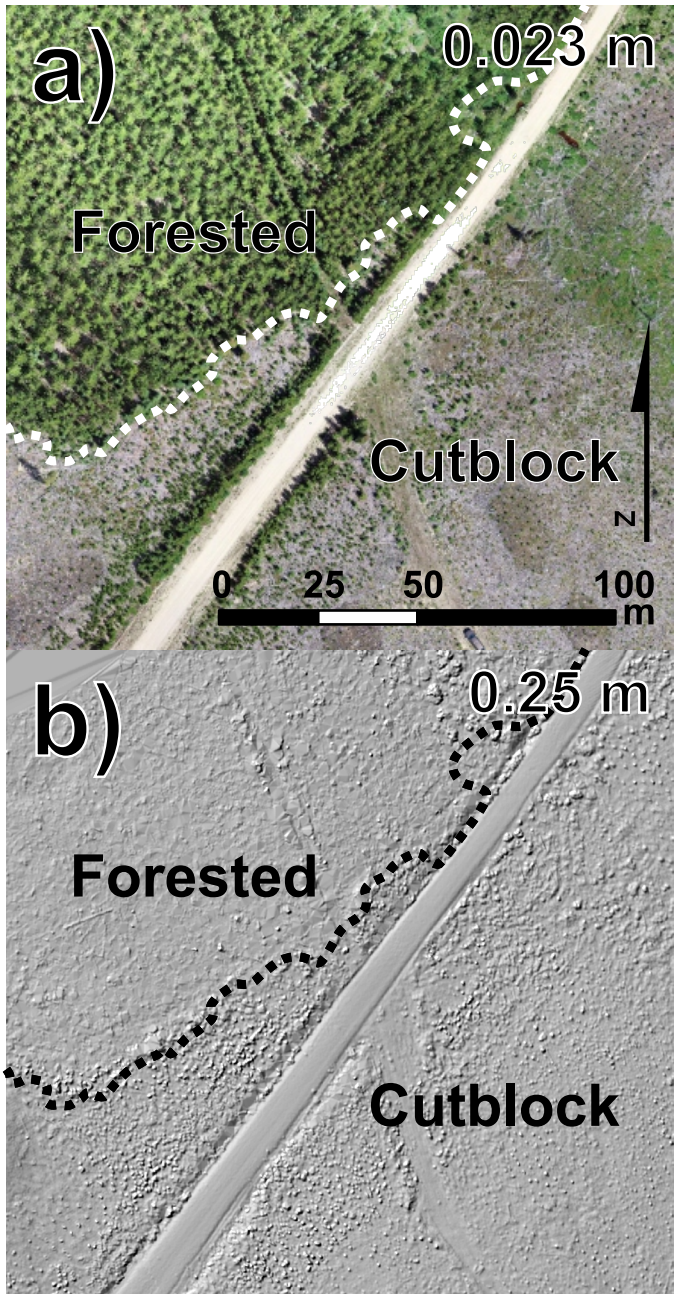

Fig. 6. Comparison of RGB imagery and lidar hillshade model at site 22EEL0003 (Skuhost Creek) with a forested area and a cutblock. **a)** Orthomosaic at 0.023 m spatial resolution produced from RPAS air photos. **b)** Lidar hillshade model at 0.25 m spatial resolution produced from ground-classified lidar points using an illumination azimuth of 315° and altitude (angle of Sun above the horizon) of 45°.

the resolution increases to 0.5 m (Fig. 5b) and 0.25 m (Fig. 5c), the margins of the drainage ditches become shaper and ruts produced by vehicle tires become apparent. About 25 m east of the road, a channel (Fig. 5b) is connected to an east-west oriented drainage ditch (Fig. 5a). This channel displays a more mottled surface pattern compared to the surrounding ground surface. The margins of the channel become easier to delineate at 0.25 m resolution (Fig. 5c). However, the ability to map surficial geology remains similar between both 0.5 m and 0.25 m resolution DEMs (Fig. 5b, 5c). Spatial resolutions of 0.25 m and higher provide the ability to locate individual fallen trees, which appear as randomly oriented linear features <20 m long and <0.3 m wide (Fig. 5c). At these resolutions, small ~0.3 m x 0.3 m points elevated above the ground surface occur throughout areas unmodified by human activities that are likely produced from boulders, stumps, or low-lying vegetation. At 0.1 m resolution, the number of these features in the hillshade model does not increase compared to 0.25 m resolution. At 0.1 m resolution, artifacts oriented perpendicular (northeast-southwest) to the flight line direction, produced from the scanning motion of the laser emitter, are visible (Fig. 5d). Artifacts and non-geological or non-geomorphological features that are accentuated at these higher spatial resolutions (0.1 m or higher) make geomorphological differences harder to resolve and do not improve the ability to map surficial geology. We found that products between 0.25 m and 0.5 m resolution provide adequate and consistent products for mapping.

5. Surficial geology maps

We mapped the surficial geology of the Sausser Lake site (21TFE0003) at a scale of 1:5,000 using 0.25 m spatial resolution lidar hillshade models and DEMs with a minimum polygon size of ~175 m^2 (Fig. 7). The survey area, centred on a recent cutblock with minimal vegetation regrowth, contains individual mature trees (>20 m high) and forest stands of moderate density that have minor effects on the density and distribution of lidar ground points. Lidar point density drops slightly in the northwest corner due to the increased tree and canopy density.

5.1. Map units

Ferbey et al. (2016) mapped the area at a scale of 1:50,000 with till veneer as the predominant map unit and a lacustrine unit in the northwest and southeast (Fig. 7a). The increased spatial resolution provided by the lidar data relative to the air photos used by Ferbey et al. (2016) enabled us to subdivide the till veneer into till blanket, streamlined till, glaciofluvial veneer, and anthropogenic units (Fig. 7b). In addition, we were able to map the edges of the lacustrine unit in greater detail. We mapped till blankets where streamlined features, which display subtle linear differences in topography, were not visible. Till units are cut by glaciofluvial sands and gravels that appear on lidar DEM to define a branching network of low-relief (~1-2 m) meltwater channels which, in the field, might be considered to reflect variations in a till blanket. On the DEM, the areas of lacustrine sediments appear as horizontal to sub-horizontal surfaces with sparse fallen trees; using lidar data alone, these deposits could have been mapped as an organic blanket without referencing the existing 1:50,000 mapping by Ferbey et al. (2016). The anthropogenic unit includes a forestry road and related drainage ditches and excavated material. Other randomly oriented, irregular, and shallow (~0.25 m) grooves cut the till blanket, streamlined till, and glaciofluvial blanket surface units. These grooves were produced by heavy logging machinery or other vehicles moving and are too small to be mapped as separate anthropogenic units.

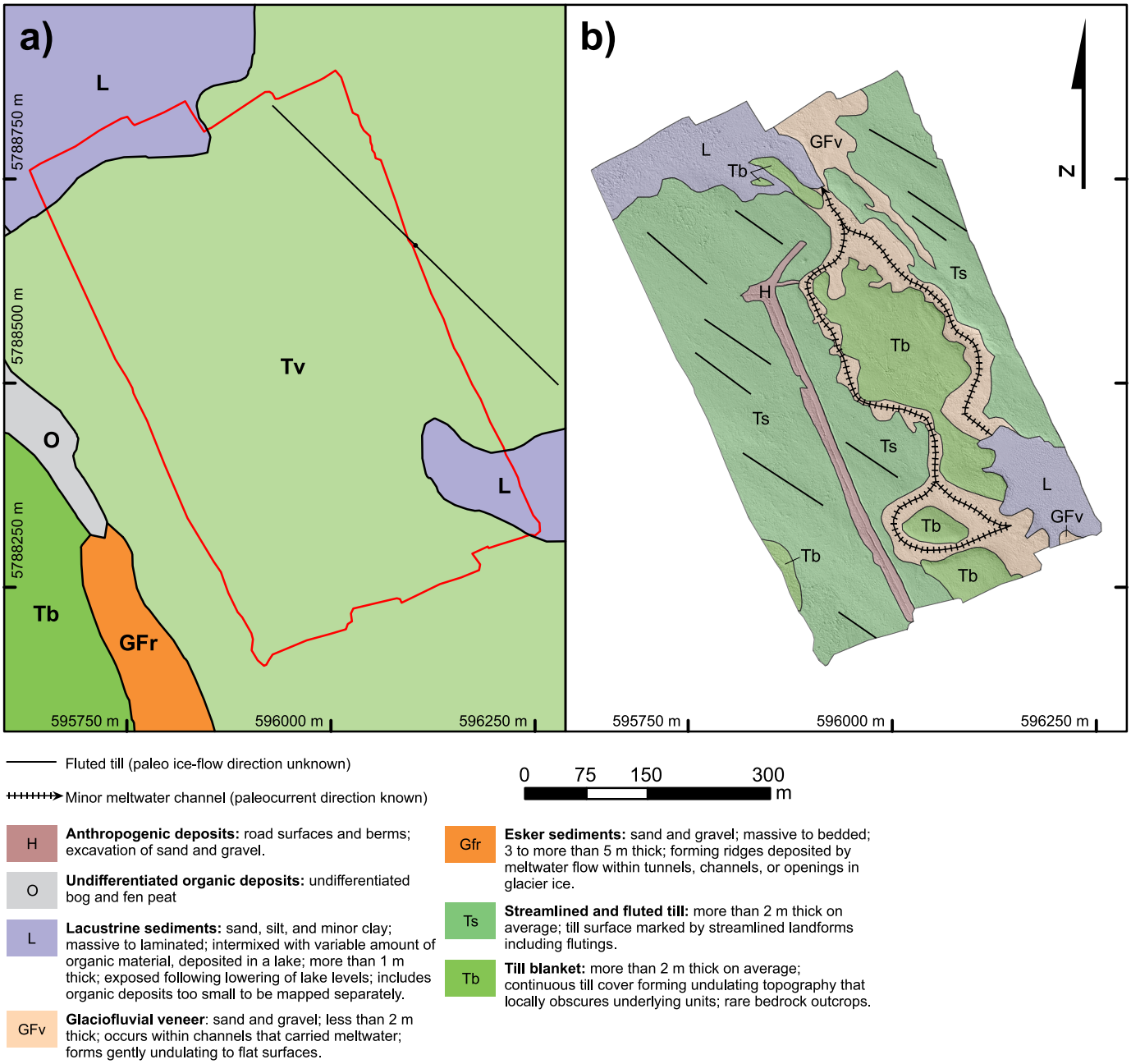

Fig. 7. Surficial geology at site 21TFE0003 (Sausser Lake). **a)** Based on 1:50,000-scale mapping by Ferbey et al. (2016). **b)** Current mapping using RPAS lidar. The orientation of bidirectional, glacially streamlined features indicates southeast-northwest ice flow. NAD83, UTM Zone 10 N.

5.2. Glacially streamlined landforms

Elongate sediment ridges (flutes) and troughs, <200 m long and <10 m wide, are distributed across the 21TFE0003 survey area, defining a glacially streamlined terrain (Figs. 7, 8). With an orientation of ~125°/305°, these bidirectional features are consistent with the regional ice flow as defined by Ferbey et al. (2016). Striations oriented 305°/125°, also consistent with regional ice flow, are exposed about 750 m southeast of the 21TFE0003 survey; these striae crosscut a second set oriented 328°/152° (Fig. 9). This earlier direction is not preserved in the landform-scale features seen in lidar DEMs and hillshade models. At other locations (e.g., 22EEL0002, Spaist Mountain, Fig. 1), we observed sediment ridges extending from bedrock outcrop aligned with regional ice flow in what we interpret as crag-and-tail landforms with a stoss and lee asymmetry yielding a unidirectional ice flow direction.

In many instances, streamlined landforms are better identified using a combination of DEM and hillshade models. For example, features oriented at 315°, a common illumination angle, can be completely missed in hillside models (Chandler et al., 2018) and, without a DEM, subtle topographic changes cannot be measured quantitatively (Fig. 7). Because the DEM enables visualizing subtle changes in topography and does not rely on shading properties like azimuth direction and altitude

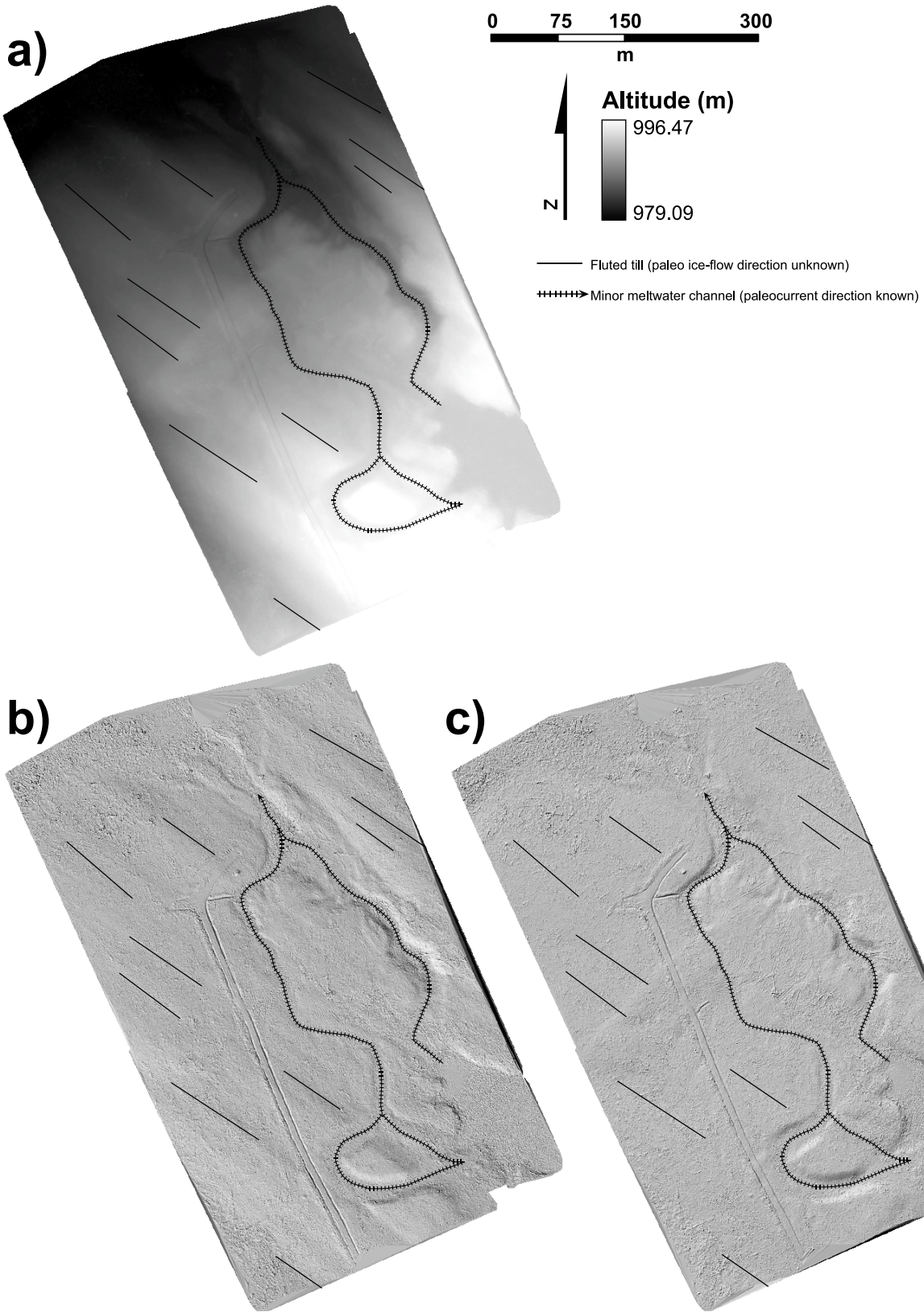

Fig. 8. DEM and hillshade for site 21TFE0003 (Sausser Lake) over streamlined till (cf. Fig. 7). All models have spatial resolutions of 0.25 m. **a)** Lidar DEM processed using Cloud Compare. **b)** Lidar hillshade model produced from the DEM using an illumination azimuth of 225° and altitude of 45°. **c)** Lidar hillshade model produced from the DEM using an illumination azimuth of 315° and altitude (angle of Sun above the horizon) of 45°.

Fig. 9. Two sets of striations on an outcrop of Chilcotin Group basalt (Miocene). The set oriented 152/328° are crosscut by the set oriented 125/305°. The outcrop is ~750 m northwest of survey area 21TFE0003 (Sausser Lake), on a flat topographic high, at 1000 m asl.

(angle of Sun above the horizon), incorporating DEM (Fig. 8) resolves the problem. For DEMs, colour ramping is important because it may enhance or diminish the expression of a feature. Lidar representations that extend across large areas with significant regional relief may not immediately show small features with subtle relief and may require re-ramping colours used to highlight landscape patterns.

5.3. Bedrock

At the Spaist Mountain site (22EEL0002), we mapped bedrock using the 0.02 m spatial resolution orthomosaic, which enabled us to identify outcrops as small as 5 m^2 (Fig. 10a). To determine if these outcrops can be identified using the lidar product alone, we superimposed locations onto a lidar hillshade (Fig. 10b). In the hillshade model, the large well-exposed outcrop (solid red outline) in the west-central part of the image exhibits a coarse, angular and mottled pattern compared to the smoother surrounding sediment, which we attribute to fracturing of the bedrock surface creating vertical contrast over small distances. Other outcrops mapped from orthomosaic imagery (dashed red outlines) are partially buried or are marked by rubbly exposures that are level with the sediment surface and do not show the same angular pattern. The smaller areas of outcrop cannot be differentiated from the sediment surface in the lidar hillshade models and cannot be confidently mapped using lidar data alone.

6. Discussion

6.1. Applications

High spatial resolution RPAS lidar DEMs (e.g., 0.50 m), enable users to discern subtle changes in topography that might be challenging or impossible to recognize on the ground or in air photos. Identifying the features related to these subtle changes may be significant for establishing the ice-flow history of an area, an important aspect of drift prospecting (e.g., Hashmi et al., 2015b; Plouffe and Ferbey, 2019). For example, parts of till blankets and veneers in areas mapped at a 1:50,000 scale may be more accurately redefined as streamlined till, such as in the present case (Fig. 7). Details from RPAS lidar may also

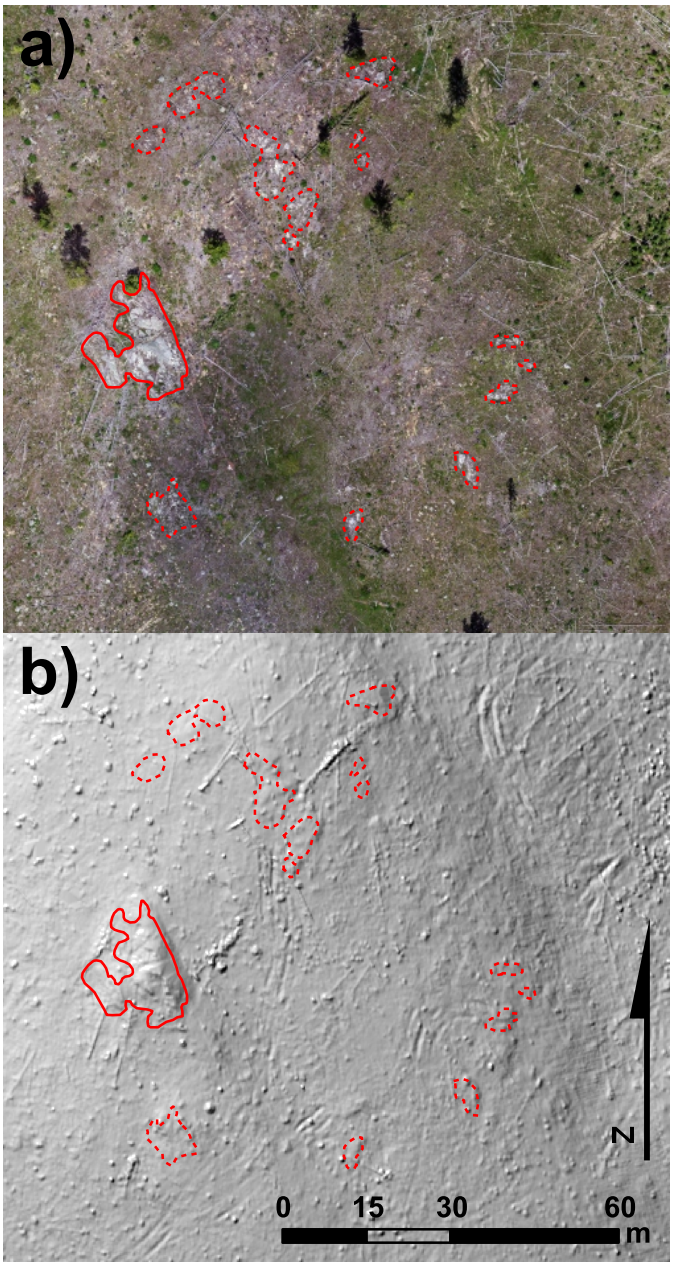

Fig. 10. Bedrock outcrop mapped at site 22EEL0002 (Spaist Mountain); ice flow is towards the southeast. Areas outlined in red dashed lines represent bedrock outcrop mapped from orthomosaic imagery. Solid red line represents large outcrop exhibiting unique topography. **a)** orthomosaic imagery with a 0.02 m spatial resolution. **b)** lidar hillshade model with a 0.25 m spatial resolution produced using an illumination azimuth of 315° and altitude of 45°.

help to better understand complex sediment transport in areas of multiple glacial advances, reversals, or ice sheet interactions and may be useful to more readily identify basal tills, the favoured medium for till geochemical and mineralogical surveys (e.g., Ferbey, 2014), and recognize post-basal till depositional processes or anthropogenic activities. In heavily drift-covered areas, RPAS lidar data can also help identify bedrock exposures or where bedrock is likely to be near the surface, such as at the stoss sides of crag-and-tail landforms.

High enough resolutions may allow measuring the orientation of bedrock structures like bedding remotely (Cracknell et al., 2013). Lidar sensors mounted on gimbals are better suited to image inclined and vertical surfaces and may provide images of inaccessible exposures on cliffs and mountainsides remotely. RPAS can acquire elevation data directly following mass movement events (Pellicani et al., 2019) or forest fires (Samiappan et al., 2019), providing an inexpensive way to update geomorphological conditions relative to existing air photos.

6.2. Accuracy

To improve lidar acquisition and processing time, we did not collect ground control point data, resulting in a sacrifice of absolute spatial accuracy relative to real-world coordinates in the final products. For our purposes, the sacrifice is justifiable because an increase would not change our map interpretations. However, the accuracy of our lidar products would likely be unacceptable for geotechnical engineering projects, which require cm-scale levels.

6.3. Limitations

To survey larger areas with our current configuration, multiple surveys must be flown separately and merged after collection. The methods used in this study cannot be applied to continuously survey large areas (e.g., >2 km^2) efficiently due to legal restrictions and hardware limitations. Transport Canada requires the RPAS to remain within visual line of sight. A DJI M600 can be tracked by a pilot or observer <~1 km away, so the theoretical maximum rectangular survey size would be ~2 km^2. Pilots can apply to Transport Canada for a special flight operations certificate to fly beyond visual line of sight, although flights would still be limited by the need for battery recharging. Upgrading to a hybrid electric or fuel-powered aircraft would increase flight times which, in combination with a special flight operations certificate, would allow broader survey areas.

The LiAir V70 data does not fully penetrate densely forested areas as it can only capture three returns; commonly these are not reflections from the ground surface. RPASs with a larger payload capacity can lift heavier lidar sensors like the DraganFly long-range lidar (DraganFly, 2023), which can measure more returns and produce denser ground point clouds in forested regions leading to increased mapping ability.

Depending on the survey conditions including the pilot's and observer's vantage point, forest conditions, and bedrock expression (e.g., glacially polished rock vs. highly fractured) RPAS lidar methods may be less effective than traditional exploration or mapping techniques.

7. Conclusion

We collected lidar data at 13 locations in the Interior Plateau at the Woodjam, Mount Polley, and Guichon Creek batholith areas using a DJI Matrice 600 hexacopter and a GreenValley LiAir V70 lidar instrument. Lidar DEMs and hillshade models with spatial resolutions of 0.25-0.5 m in forested and clearcut areas were produced from data collected at 80-100 m above ground level, at 4-5 m/s. RPAS lidar enables observation of surface expressions too subtle to be expressed in traditional air photos or in the field, including the delineation of fluted terrain and crag-and-tail landforms related to regional ice flow. Using hillshade models and DEMs, we were able to map a range of surficial material types including till, glaciofluvial, anthropogenic, colluvium, and bedrock in detail, over areas as small as 100 m^2. Results from this study establish exchangeable payload aircraft as an affordable platform for acquiring topographic data in the field to help map surficial geology. Improvements to the lidar sensor and its ability to receive more returns would increase ground-point densities within forested areas and produce DEMs with a more consistent ability to map across changing forest and vegetation conditions.

Acknowledgements

We thank W. Morton and B. Laird (Consolidated Woodjam Copper Corp.), J. Miller-Tait, C. Rees, and G. Roste (Mount Polley Mining and Imperial Metals corporations), and M. Cathro and G. Newton (Happy Creek Minerals Ltd.), for access to properties and insights into local geology. K. Linkevičs and A. Dobrovolskiy (SPH Engineering) provided technical advice and support on survey design and implementation. A special thanks go to M. Sakals (British Columbia Ministry of Forests, Lands, Natural Resource Operations) and J. Thompson (British Columbia Ministry of Water, Land, and Resource Stewardship) for their guidance and knowledge in adopting remotely piloted aircraft systems into our field surveys. We greatly benefited from the time spent in the field with J. Heshi and C. Wildgust (Candrone) and the knowledge they shared. J. Van Der Vlugt, K. Zaborniak, and C. Fielding (BCGS) assisted capably in the office and the field. The article benefitted from a critical review by Sophie Norris (University of Victoria).

References Cited

Alsadik, B., and Remondino, F., 2020. Flight planning for lidar-based UAS mapping applications. ISPRS International Journal of GeoInformation, 9, 378p. https://doi.org/10.3390/ijgi9060378

British Columbia Ministry of Forests, 2023. Digital air photos of B.C. Province of British Columbia. https://www2.gov.bc.ca/gov/content/data/geographic-data-services/digital-imagery/air-photos (accessed August 2023).

Chandler, B.M.P., Lovell, H., Boston, C.M., Lukas, S., Barr, I.D., Benediktsson, Í.Ö., Benn, D.I., Clark, C.D., Darvill, C.M., Evans, D.J.A., Ewertowski, M.W., Loibl, D., Margold, M., Otto, J.-C., Roberts, D.H., Stokes, C.R., Storrar, R.D., and Stroeven, A.P., 2018. Glacial geomorphological mapping: A review of approaches and frameworks for best practice. Earth-Science Reviews, 185, 806–846. https://doi.org/10.1016/j.earscirev.2018.07.015

Clague, J.J., and Ward, B.C., 2011. Pleistocene glaciation of British Columbia. In: Ehlers, J., Gibbard, P.L., and Hughes, P.D. (Eds.) Developments in Quaternary Sciences Volume 15, pp. 563-573 https://doi.org/10.1016/B978-0-444-53447-7.00044-1

Cracknell, M.J., Roach, M., Green, D., and Lucieer, A., 2013. Estimating Bedding Orientation From High-Resolution Digital Elevation Models. IEEE Transactions on Geoscience and Remote Sensing, 51, 2949-2959. https://doi.org/10.1109/TGRS.2012.2217502

Deblonde, C., Cocking, R.B., Kerr, D.E., Campbell, J.E., Eagles, S., Everett, D., Huntley, D.H., Inglis, E., Parent, M., Plouffe, A., Robertson, L., Smith, I.R., and Weatherston A., 2019. Surficial data model: the science language of the integrated Geological Survey of Canada data model for surficial geology maps. Geological Survey of Canada Open File 8236, 11p.

Demchuk, T.E., Ferbey, T., Kerr, B.J., and Levson, V.M., 2005. Surficial geology and aggregate potential mapping in northeast British Columbia using lidar imagery. In: Summary of Activities 2005, British Columbia Ministry of Energy and Mines, pp. 51-59.

Diakow, L.J., Newell, J.M., and Metcalfe, P., 1997. Interior Plateau geoscience project: summary of geological, geochemical and geophysical studies. British Columbia Ministry of Employment and Investment. British Columbia Geological Survey Paper 1997-2, 256p.

DraganFly, 2023. Long Range LiDAR. DraganFly. https://draganfly.com/lidar/ (accessed August 2023).

Elia, E.A., and Ferbey, T., 2020. Generating photogrammetric DEMs in the field from remotely piloted aircraft systems. In: Geological Fieldwork 2019, British Columbia Ministry of Energy, Mines and Petroleum Resources, British Columbia Geological Survey Paper 2020-01, pp. 189-200.

Elia, E.A., Ferbey, T., Ward, B.C., Shives, R.B.K., Best, M., and Martin-Burtart, N., 2023. Remotely piloted aircraft system (RPAS) for investigating surface sediments in the Interior Plateau of British Columbia: Methods, data, and products. British Columbia Ministry of Energy, Mines and Low Carbon Innovation, British Columbia Geological Survey GeoFile 2023-07, 22p.

Ferbey, T., 2014. Basal till potential of the Colleymount map area (NTS 093L/01), British Columbia. British Columbia Ministry of Energy and Mines, British Columbia Geological Survey Open File 2014-04, 1:50,000 scale.

Ferbey, T., Levson, V.M., and Plouffe, A., 2016. Surficial geology, Moffat Creek area, British Columbia, parts of NTS 93-A/3, NTS 93-A/4, NTS 93-A/5, and NTS 93-A/6. British Columbia Ministry of Energy and Mines, British Columbia Geological Survey Geoscience Map 2016-01, 1:50,000 scale

Ferbey, T., Elia, E.A., Shives, R.B.K., Martin-Burtart, N., Best M., and Ward, B.C., 2024. Quantifying potassium concentrations in Interior Plateau surface sediments using remotely piloted aircraft system gamma-ray spectrometry. British Columbia Ministry of Energy, Mines and Low Carbon Innovation, British Columbia Geological Survey Open File in press.

GreenValley International, 2017. LiAir V70: UAV lidar system user guide, 41p. https://greenvalleyintl.com/static/upload/file/20210716/1626437614111663.pdf

Hashmi, S., Plouffe, A., and Ward, B.C., 2015a. Surficial geology of Bootjack Mountain area, parts of NTS 93-A/5, NTS 93-A/6, NTS 93-A/11, and NTS 93-A/12. British Columbia Ministry of Energy and Mines, British Columbia Geological Survey Geoscience Map 2015-02, 1:50,000 scale.

Hashmi, S., Ward, B.C., Plouffe, A., Leybourne, M.I., and Ferbey, T., 2015b. Geochemical and mineralogical dispersal in till from the Mount Polley Cu-Au porphyry deposit, central British Columbia, Canada. Geochemistry: Exploration, Environment, Analysis, 15, 234-249.

Holland, S.S., 1976. Landforms of British Columbia: a physiographic outline. British Columbia Ministry of Energy and Mines, and Petroleum Resources, British Columbia Geological Survey Bulletin 48, 138p.

Kerr, D.E., and Levson, V.M., 1997. Drift prospecting activities in British Columbia: an overview with emphasis on the Interior Plateau. In: Diakow, L.J., and Newell, J.M., (Eds.) Interior Plateau Mapping Project: Summary of Geological, Geochemical and Geophysical Studies. British Columbia Ministry of Employment and Investment, British Columbia Geological Survey Paper, 1997-2, pp. 159-172.

Lemmens, M., 2007. Airborne lidar sensors. GIM International, Product Survey, 4p. https://community.esri.com/ccqpr47374/attachments/ccqpr47374/gis-blog/507/1/LiDAR-Sensors.pdf

LidarBC, 2024. Open LiDAR Data Portal. https://lidar.gov.bc.ca/pages/download-discovery (accessed March 2024).

Logan, J.M., 2013. Porphyry systems of central and southern BC: Overview and field trip road log. In: Logan, J., and Schroeter, T.G., (Eds.), Porphyry Systems of Central and Southern BC: Prince George to Princeton. Society of Economic Geologists Field Trip Guidebook Series 44, pp. 1-45.

Lohani, B., and Ghosh, S., 2017. Airborne LiDAR technology: A review of data collection and processing systems. Proceedings of the National Academy of Sciences, India Section A: Physical Sciences, 87, 567-579. https://doi.org/10.1007/s40010-017-0435-9

Maune, D.F., Heidemann, H.K., Kopp, S.M., and Crawford, C.A., 2018. Introduction to digital elevation models. In: Maune, D.F., Nayegandhi, A. (Eds.), Digital Elevation Model Technologies and Applications: The Dem Users Manual 3rd Edition. 3, pp. 1-40.

Nayegandhi, A., and Nimetz, J., 2018. Airborne topographic lidar. In: Maune, D.F., and Nayegandhi, A. (Eds.), Digital Elevation Model Technologies and Applications: The Dem Users Manual 3rd Edition. 3, pp. 205-236.

Pellicani, R., Argentiero, I., Manzari, P., Spilotro, G., Marzo, C., Ermini, R., and Apollonio, C., 2019. UAV and airborne lidar data for interpreting kinematic evolution of landslide movements: The case study of the Montescaglioso landslide (Southern Italy). Geosciences, 9, article 9060248. https://doi.org/10.3390/geosciences9060248

Plouffe, A., and Ferbey, T., 2016. Till geochemistry, mineralogy and textural data near four Cu porphyry deposits in British Columbia. British Columbia Ministry of Energy and Mines, British Columbia Geological Survey GeoFile 2016-10, 44p.

Plouffe, A., and Ferbey, T., 2017. Porphyry Cu indicator minerals in till: A method to discover buried mineralization. In: Ferbey, T., Plouffe, A., and Hickin, A.S., (Eds.), Indicator Minerals in Till and Stream Sediments of the Canadian Cordillera. Geological Association of Canada Special Paper Volume 50, and Mineralogical Association of Canada Topics in Mineral Sciences Volume 47, pp. 129-159.

Plouffe, A., and Ferbey, T., 2018. Surficial geology of the Highland Valley copper mine area (Parts of NTS 092I/06, 7, 10 and 11), British Columbia., British Columbia Ministry of Energy and Mines, British Columbia Geological Survey Geoscience Map 2018-01, 1:50,000 scale.

Plouffe, A., and Ferbey, T., 2019. Indicator-mineral content of bedrock and till at the Gibraltar porphyry Cu-Mo deposit and the Woodjam porphyry Cu-Au-Mo prospect, south-central British Columbia. British Columbia Ministry of Energy, Mines and Petroleum Resources, British Columbia Geological Survey Open File 2019-10, 33p.

Samiappan, S., Hathcock, L., Turnage, G., McCraine, C., Pitchford, J., and Moorhead, R., 2019. Remote sensing of wildfire using a small unmanned aerial system: Post-fire mapping, vegetation recovery and damage analysis in Grand Bay, Mississippi/Alabama, USA. Drones, 3, article 3020043. https://doi.org/10.3390/drones3020043

Zhang, W., Qi, J., Wan, P., Wang, H., Xie, D., Wang, X., and Yan, G., 2016. An easy-to-use airborne lidar data filtering method based on cloth simulation. Remote Sensing, 8, article 8060501. https://doi.org/10.3390/rs8060501

BRITISH COLUMBIA

Ministry of
Energy, Mines and
Low Carbon Innovation

BRITISH COLUMBIA
est. 1895
GEOLOGICAL SURVEY